Band-Edge Oscillator Strength of Colloidal CdSe/CdS Dot-in-Rods: Comparison of Absorption and Time-Resolved Fluorescence Spectroscopy

–

Electronic Supplementary Information (ESI)

I. Angeloni,[a,b] W. Raja,[a,c] A. Polovitsyn,[a,b] F. De Donato,[a] R. Proietti Zaccaria,[a,*] and I. Moreels[a,*]

[a] *Istituto Italiano di Tecnologia, via Morego 30, IT-16163 Genova, Italy.*

[b] *Dipartimento di Chimica e Chimica Industriale, Università di Genova, Via Dodecaneso 33, IT-16146 Genova, Italy*

[c] *Dipartimento di Fisica, Università di Genova, Via Dodecaneso 33, IT-16146 Genova, Italy*

* iwan.moreels@iit.it; Remo.Proietti@iit.it

1. Materials properties

Table S1. CdSe/CdS DiRs

	sample name	core diameter (nm)	total diameter (nm)	AR	QE (%)	Abs peak E_0 (eV)	PL peak (eV)	FWHM band edge (meV)*
CdSe/CdS DIRs	NR1	2.1	5.1	8.7	78.82	2.09	2.06	86.7
	NR2	2.8	4.8	14.5	80.82	2.13	2.08	109
	NR3	3.3	4.2	9.6	35.7	2.08	2.05	73.5
	NR4	3.3	4.3	9.8	61.35	2.07	2.04	75.1
	NR5	3.4	5.3	5.3	31.72	2.07	2.03	88.8
	NR6	3.4	4.3	7.2	67.26	2.10	2.07	85.1
	NR7	3.4	5.0	6.2	26.25	2.07	2.04	87.0
	NR8	3.4	4.7	7.9	65.65	2.08	2.05	76.5
	NR9	3.5	5.5	5.9	72.85	2.06	2.03	80.2
	NR10	3.5	5.9	4.4	75.84	2.05	2.01	81.5
	NR11	3.5	4.6	21.3	48.96	2.06	2.03	90.6
	NR12	3.7	5.5	5.1	78.93	2.05	2.01	94.1
	NR13	3.7	6.1	2.0	58.81	2.05	2.01	83.3
	NR14	4.3	6.3	2.4	48.89	2.01	1.97	84.7
	NR15	4.7	5.8	6.4	76.70	1.97	1.94	85.2
	NR16	4.7	6.6	3.9	68.55	1.97	1.93	78.7
	NR17	4.7	7.0	4.2	70.72	1.96	1.92	87.6
	NR18	4.8	6.0	6.4	83.40	1.97	1.93	73.3
	NR19	4.8	5.4	4.7	53.94	1.98	1.94	79.5
	NR20	5.2	5.9	2.5	61.55	1.96	1.93	67.7
	NR21	5.2	6.2	2.3	41.24	1.97	1.94	80

	NR22	5.6	6.6	3.8	2.85	1.93	-	-
	NR23	5.7	6.2	4.2	70.92	1.93	1.90	74.6

*The FWHM values of the band edge transition were calculated from the low-energy side of the absorption spectra.

Table S2. CdSe cores

	sample name	core diameter (nm)	abs. peak E_0 (eV)
CdSe QDs	QD1	2.3	2.53
	QD2	2.5	2.44
	QD3	2.7	2.37
	QD4	2.7	2.36
	QD5	2.9	2.33
	QD6	3.0	2.29
	QD7	3.4	2.22
	QD8	3.9	2.15
	QD9	4.2	2.11
	QD10	4.3	2.09
	QD11	4.7	2.06
	QD12	4.8	2.05
	QD13	5.8	1.98
	QD14	6.1	1.97

2. Local field factor

2.1. Analytical calculation of the local field factor for the CdSe QDs

To calculate the local field factor in the case of spherical particles, we started from the general expression of the polarizability of a coated sphere:[1]

$$\alpha = \frac{V\left(\left(\varepsilon_{lig} - \varepsilon_s\right)\left[\varepsilon_{lig} + \left(\varepsilon_{CdSe} - \varepsilon_{lig}\right)(L - fL)\right] + f\varepsilon_{lig}\left(\varepsilon_{CdSe} - \varepsilon_{lig}\right)\right)}{\left(\left[\varepsilon_{lig} + \left(\varepsilon_{CdSe} - \varepsilon_{lig}\right)(L - fL)\right]\left[\varepsilon_s + \left(\varepsilon_{lig} - \varepsilon_s\right)L\right] + fL\varepsilon_{lig}\left(\varepsilon_{CdSe} - \varepsilon_{lig}\right)\right)} \qquad (1)$$

Here, V is the total volume of the particle, $\varepsilon_{lig} = n_{lig}^2$ is the dielectric constant of the ligand coating, ε_{CdSe} is the complex dieletric function of CdSe, $\varepsilon_s = n_s^2$ is the dielectric constant of the solvent, f is the fraction of the total volume occupied by the CdSe NC, and L is the depolarization factor, equal to 1/3. The equation above -and hence the subsequent equations- have to be evaluated both for parallel and perpendicular directions, as the wurtzite crystal structure of the NCs implies slightly different optical constants along the directions parallel and perpendicular to the NC optical axis.[2,3]

The polarizability of the coated particle is related to the absorption coefficient through:

$$\mu_i = \frac{2\pi n_s}{\lambda V} Im(\alpha) \qquad (2)$$

with $V_{CdSe} = fV$, we have to rescale μ_i by f in order to obtain the intrinsic absorption coefficient of CdSe:

$$\mu_{i,CdSe} = \frac{\mu_i}{f} = \frac{2\pi n_s}{\lambda V_{CdSe}} Im(\alpha) \quad (3)$$

Considering that the same quantity can be expressed as:[4]

$$\mu_{i,CdSe} = \frac{2\pi}{\lambda n_s} |f_{LF}|^2 Im(\varepsilon_{CdSe}) \quad (4)$$

comparison of equations (3) and (4) yields:

$$|f_{LF}|^2 = \frac{n_s^2 Im(\alpha)}{V_{CdSe} Im(\varepsilon_{CdSe})} \quad (5)$$

For a CdSe core diameter of 3 nm and a ligand shell length of 1.8 nm, $|f_{LF,||}|^2 = 0.345$ and $|f_{LF,\perp}|^2 = 0.350$ have been calculated. The dielectric function of ligands, CdSe and the solvent are the same used in the simulation of the DiRs, which are reported in the main text.

2.2. Influence of the core position in DiRs

The influence of the core position on the local electric field $\boldsymbol{E}_{loc}$ in the CdSe core was evaluated with a finite element simulation (AR=4, total diameter: 5.5 nm, core diameter: 4 nm), varying the core position from 10% to 50% of the total rod length. The strong enhancement that $\boldsymbol{E}_{loc}$ experiences in the direction parallel to the long axis of the rod is partly compensated for by a concomitant reduction along the perpendicular directions, resulting in an overall 15% increase in $|f_{LF}|^2$ when moving the core position from 10% to 50% of the rod length.

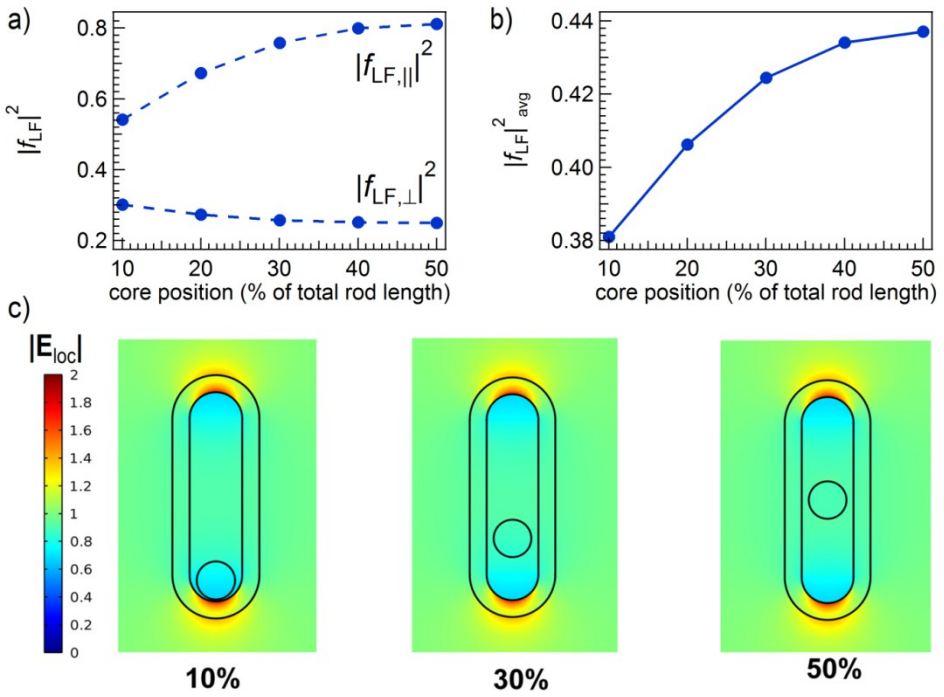

Figure S1. Dependence of f_{LF} on the core position along the rod. a) Parallel and perpendicular components of f_{LF} and b) average f_{LF}. c) Simulated electric field magnitude along the NC ($\boldsymbol{E}_{ext}$ parallel to the NC long axis) in three representative cases. When moving the core towards the center of the rod, it experiences a higher $\boldsymbol{E}_{loc}$.

3. Comparison of CdSe QDs f_{gap} with literature

In the work of Čapek et al.,[5] the local field factor at the band edge is calculated according to:[6]

$$|f_{LF}|^2 = \frac{9n_s^4}{\left(n^2 - k^2 + 2n_s^2\right)^2 + 4(nk)^2} \qquad (6)$$

with n_s = 1.445, n and k the real and imaginary part of the bulk dielectric function of zincblende CdSe[7] and the assumption of $k<<n$. The resulting $|f_{LF}|^2$ equals 0.253. Using Equation 2 in the main text, the corresponding values for σ_{gap} are plotted (yellow squares) in Figure S2, together with our data (red triangles). The same procedure has been used to calculate σ_{gap} starting from the oscillator strength of wurtzite CdSe QDs of Jasieniak,et al.[8] (blue circles).

It is clear that all integrated cross sections agree well. The remaining small difference between our data and literature can be related to a slightly lower absorption coefficient that we measured at high energy: $2.05 \cdot 10^5$ cm^{-1} at 4.2 eV, with respect to a value of $2.3 \cdot 10^5$ cm^{-1} at 4.13 eV measured by Čapek et al.[5] (the molar extinction of Jasieniak et al.[8] is reported only at 3.54 eV). This difference translates directly into a different σ_{gap}.

For the comparison of f_{gap}, the local field factor at the band gap has also to be known. $|f_{LF}|^2$ in the case of Čapek et al.[5] equals 0.253, while we find slightly higher values (see above) due to the influence of the organic ligand shell, and the lower refractive index used. This further increases the

difference between our data and literature, finally yielding values that in our case are about 20-40% lower.

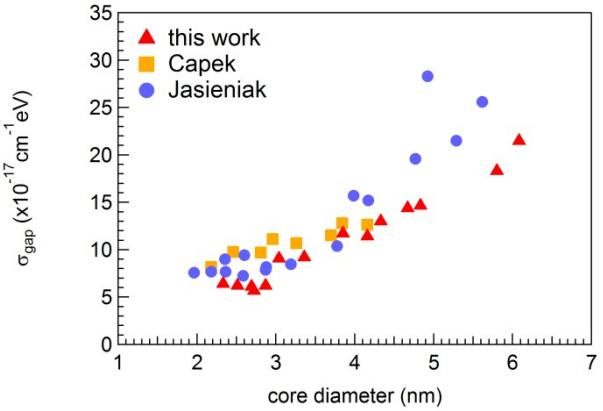

Figure S2. Absorption cross section at the band gap of our CdSe cores compared to literature data.

4. Calculation of the oscillator strength.

Considering the parallel and perpendicular components of the absorption cross section and local field factor we find (see Equation 2 in the main text):

$$f_{gap} = \frac{2\varepsilon_0 n_s c m_e}{3e^2\pi\hbar} \cdot \left(\frac{2\sigma_{\perp}}{|f_{LF,\perp}|^2} + \frac{\sigma_{||}}{|f_{LF,||}|^2} \right) \qquad (7)$$

Assuming that the oscillator strength is isotropic:

$$\frac{\sigma_{\perp}}{|f_{LF,\perp}|^2} = \frac{\sigma_{||}}{|f_{LF,||}|^2} \rightarrow \sigma_{\perp} = \sigma_{||} \cdot \frac{|f_{LF,\perp}|^2}{|f_{LF,||}|^2} \qquad (8)$$

from which

$$\sigma_{gap} = \frac{1}{3}\sigma_{||} \cdot \left(1 + 2\frac{|f_{LF,\perp}|^2}{|f_{LF,||}|^2} \right) \rightarrow \sigma_{||} = \frac{3\sigma_{gap}|f_{LF,||}|^2}{\left(|f_{LF,||}|^2 + 2|f_{LF,\perp}|^2\right)} \qquad (9)$$

and finally:

$$f_{gap,||} = f_{gap,\perp} = \frac{2\varepsilon_0 n_s c m_e}{e^2\pi\hbar} \cdot \frac{\sigma_{||}}{|f_{LF,||}|^2} = \frac{2\varepsilon_0 n_s c m_e}{e^2\pi\hbar} \cdot \frac{3\sigma_{gap}}{\left(|f_{LF,||}|^2 + 2|f_{LF,\perp}|^2\right)} \qquad (10)$$

5. Absorption peak red-shift upon shell growth.

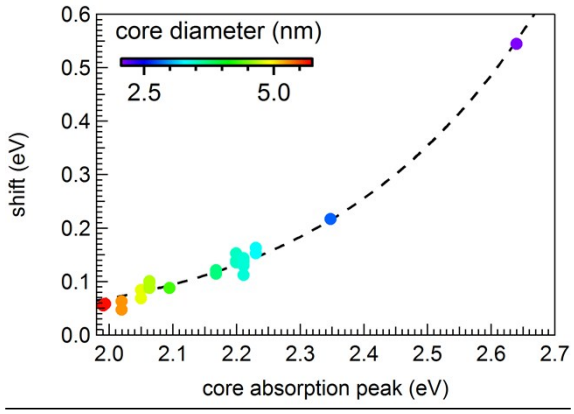

Figure S3. Shift of the first absorption peak after shell growth.

6. Dependence of the oscillator strength on DiR geometry.

No clear dependence of f_{gap} was found on NC AR, NC diameter or shell thickness, even when comparing DiRs with a similar core diameter (graphs below, core diameters are comprised between 3.3 and 3.5 nm). It confirms that, in addition to the overall geometry of the system, more subtle differences such as the core/shell interface also contribute to the electron-hole overlap. Indeed, delocalization effects only become apparent when restricting the analysis to sets of samples synthesized using the same seed (see main text).

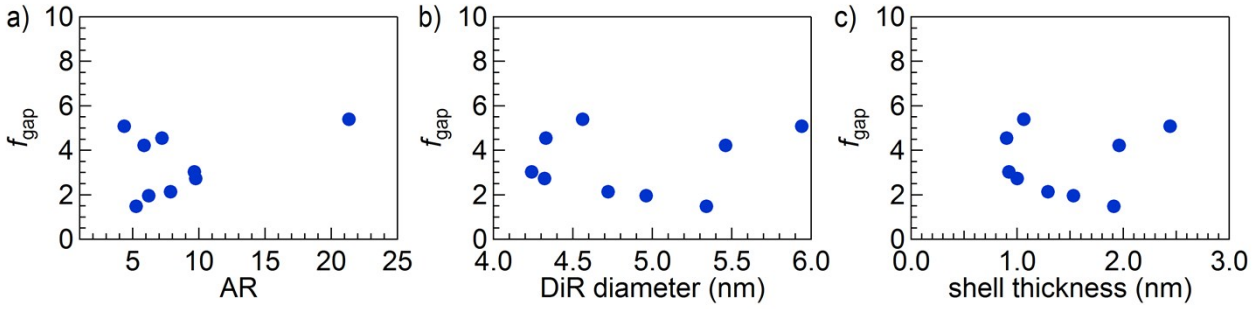

Figure S4. f_{gap} of a subset of DiRs with core diameters from 3.3 to 3.5 nm in dependence of the DiR AR (a), the DiR total diameter (b) and the shell thickness, calculated as the difference between the total and the core diameters (c).

7. Estimate of the CdS band gap

The CdS band gap was determined from the absorbance A, by fitting the linear region of the CdS absorption onset using a Tauc plot (plotting $\sqrt{A \cdot E_0}$ as a function of E_0). The estimated band gap is the intercept of the fitted line with x-axis.

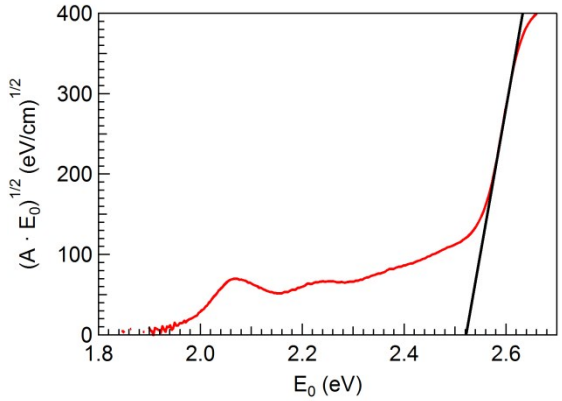

Figure S5. Tauc plot for a representative DiR (red line) and fit of the linear region of the CdS absorption onset.

8. Influence of QE on the radiative lifetime

The PL decay traces upon excitation with both 405 nm and 510 nm pulsed lasers of two more representative samples are presented in Figure S6 (see main text, Fig. 5 for the first one). Again, the appearance of a slow component when exciting the CdS shell is associated with shallow electron trapping.

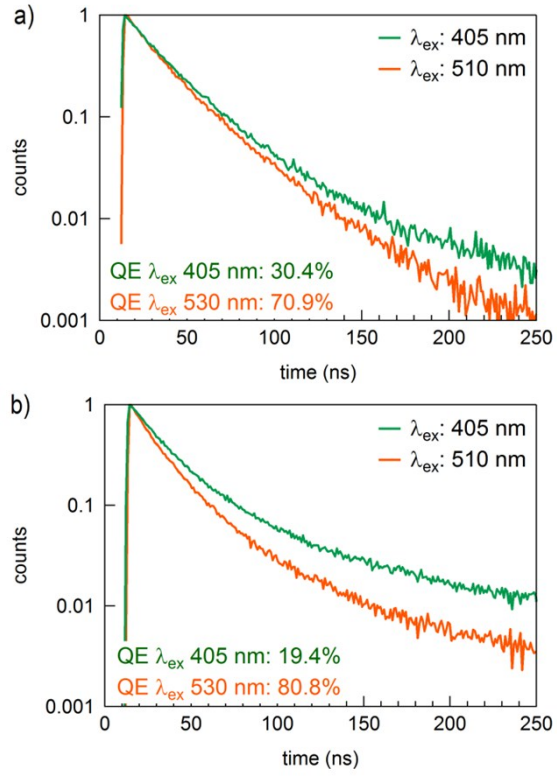

Figure S6. PL decay traces upon excitation with 405 nm (green line) and 510 nm (orange line) for samples NR23 (a) and NR2 (b) in Table S1.

Note that, in contrast with the first 2 samples, for NR2 (Figure S6b) also the radiative lifetime is somewhat reduced when exciting the sample at 510 nm.

panel	Excitation wavelength	τ_1 (w_1)	τ_2 (w_2)	τ_{rad}	τ_3 (w_3)
a)	405 nm	16.2 ns (33%)	32.4 ns (59%)	26.6 ns	183.3 ns (7%)
	510 nm	16.6 ns (49%)	31.5 ns (44%)	23.7 ns	69.6 ns (8%)
b)	405 nm	17.8 ns (48%)	56.5 ns (33%)	33.4 ns	343 ns (19%)
	510 nm	14.5 ns (53%)	34.9 ns (36%)	22.7 ns	187 ns (11%)

Table S3. Lifetime components (with respective weights) and radiative lifetime from the fits of the decays in Figure S6a and S6b.

9. Lifetime analysis

As reported in the main text, we fitted all our DiRs spectra with a sum of three exponential functions. The resulting three decay constants were ascribed to either radiative or non-radiative processes.

9.1. The fastest component (τ_1)

There is a subset of NCs whose τ_1 has a weight below 20-30% and a decay time of less than 10 ns. These NCs typically show a low PL QE. In these cases τ_1 is attributed to fast trapping, and it does not contribute to the radiative emission rate (open symbols).[9] The closed symbols on the other hand are assigned to radiative recombination, and have a significantly higher weight in the overall decay.

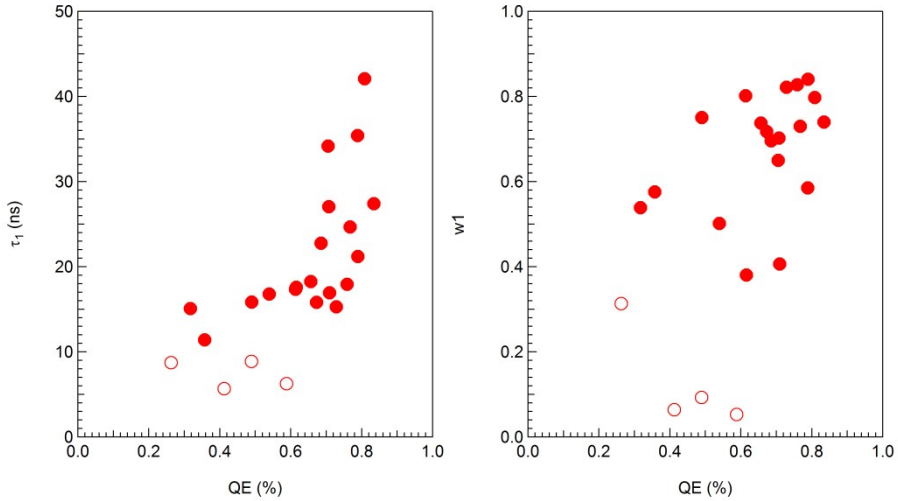

Figure S7. Fastest components versus QE. Full (empty) symbols indicate radiative (non-radiative) components.

9.2. The slowest component (τ_3)

All samples have a slow component with low weight (less than 30%). Among them, only two have a τ_3 lower than 80 ns. With a weight above 10%, we consider these to contribute to the radiative decay (full circles). For all the other datapoints, the τ_3 component is assigned to delayed emission.[9]

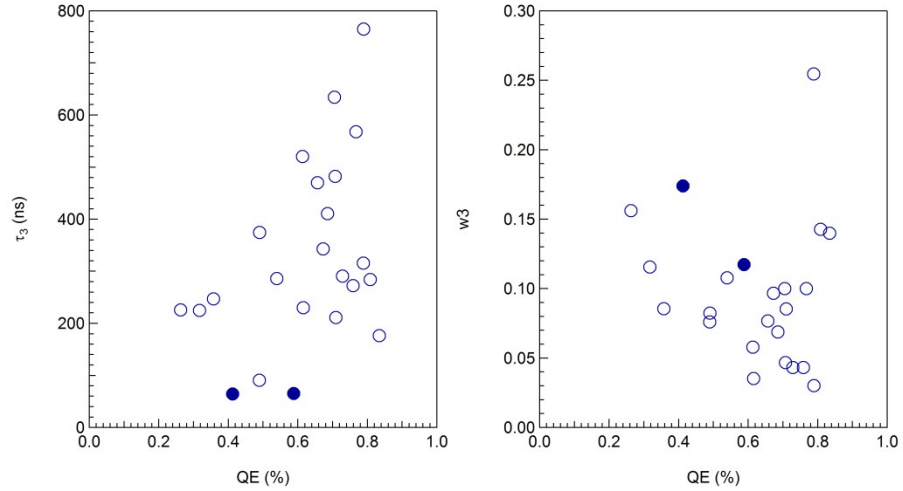

Figure S8. Slowest components versus QE. Full (empty) symbols indicate radiative (non-radiative) components.

9.3. The intermediate component (τ_2)

For nearly all samples, τ_2 can be assigned to radiative recombination, only one sample has a second component (empty circle) whose decay time and low weight is consistent with shallow trapping and delayed emission.

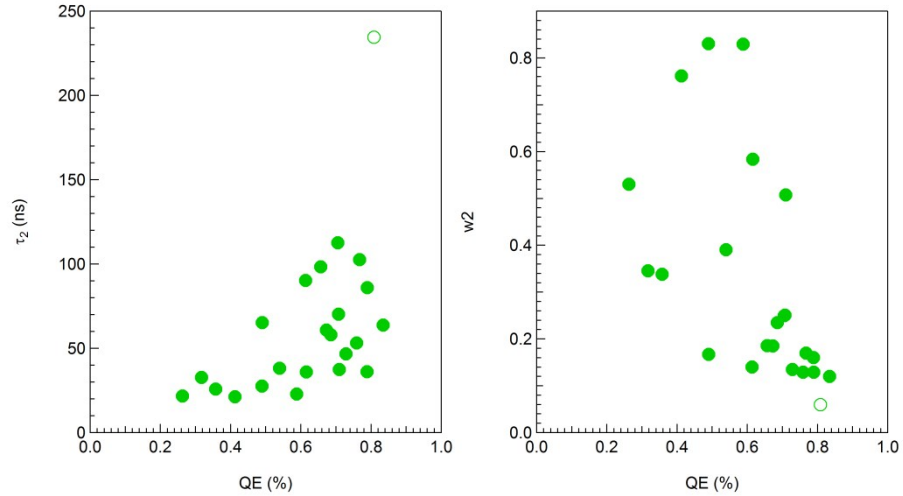

Figure S9. Intermediate components versus QE. Full (empty) symbols indicate radiative (non-radiative) components.

For a global plot of the three components, we refer the reader to the main text.

9.4. Comparison with biexponential fit

To verify if three exponential functions are needed to fit the PL decay traces, we repeated the analysis using a bi-exponential fit. Although for part of the samples the goodness of fit (χ^2) is not

significantly different when fitting with two or three exponentials, it is almost double for samples with a low quantum efficiency. Since our approach is to provide a single model to account for all samples, we decided to fit with three components.

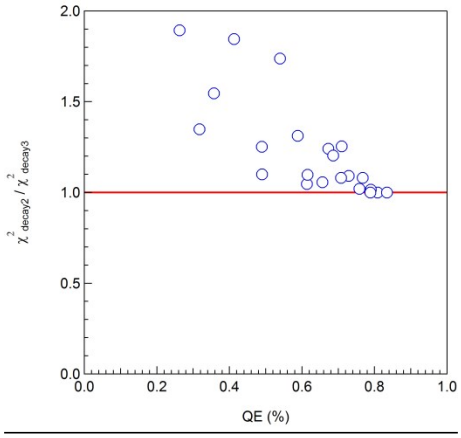

Figure S10. Ratio between the χ^2 values obtained with bi- and triexponential fits to the PL decay traces, plotted with respect to the quantum efficiency.

To compare the two approaches in terms of the radiative lifetime, we analysed the different decay components obtained from the biexponential fit in the same way as how we analysed the three-component fit. For three samples, the fastest component (Figure S11, top) was associated with fast nonradiative recombination and discarded, due to the low weight and the short time constant. Concerning the longest component (Figure S11, bottom), two samples presented a time constant longer than 250 ns, which we ascribed to delayed emission and discarded as well.

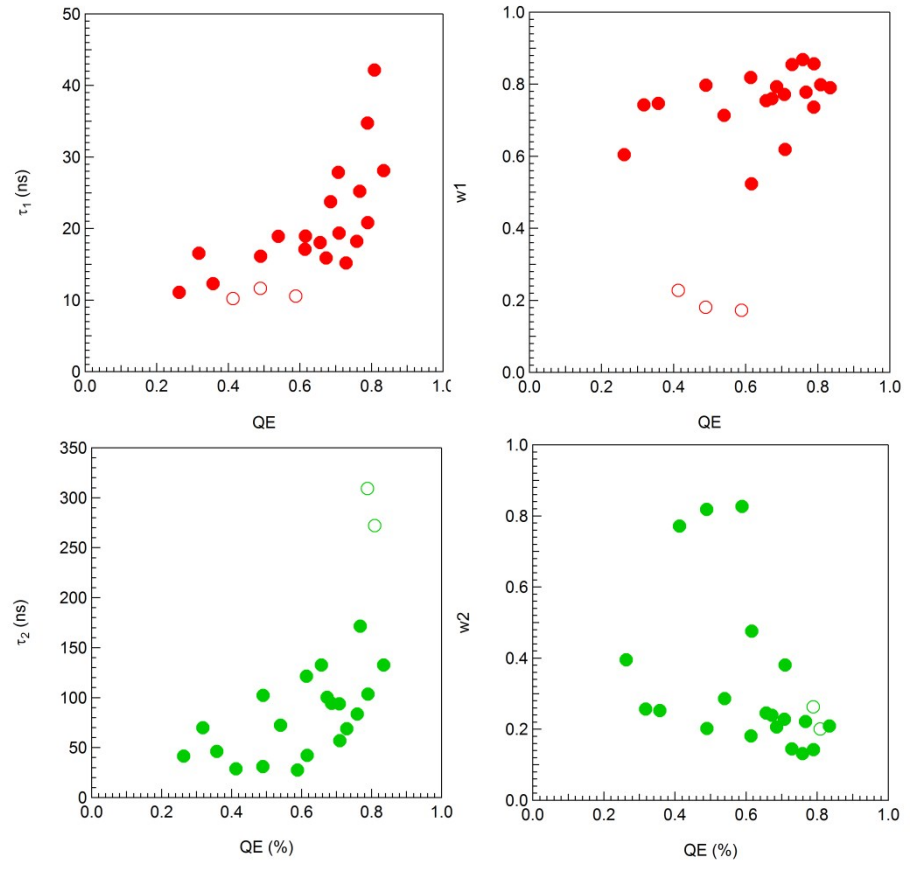

Figure S11. Short (top) and long (bottom) decay components versus QE. Full (empty) symbols indicate radiative (non-radiative) components.

A comparison of the area-weighted radiative lifetimes from biexponential (**Figure** S12a, open symbols) and triexponential (**Figure** S12a, closed symbols) fits shows that overall similar values are obtained. Note that in several cases, the biexponential fits failed to properly account for the long-lifetime component (**Figure** S12b), further supporting the need to use three components.

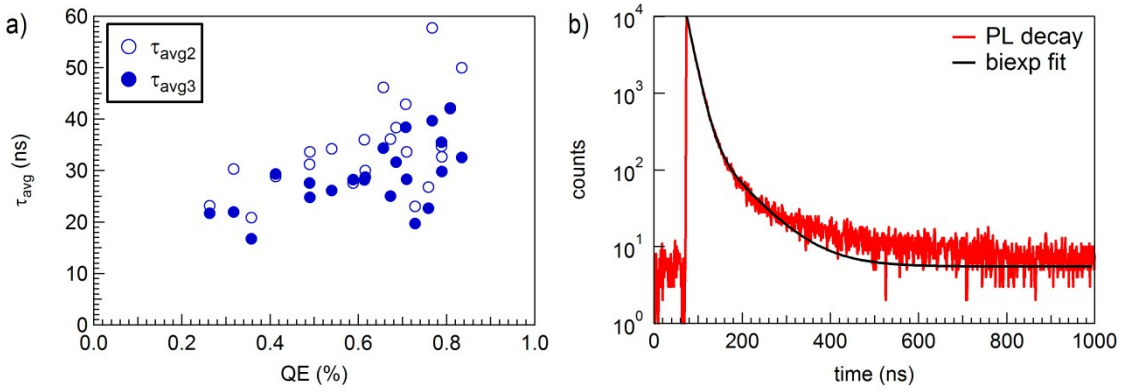

Figure S12. a) τ_{avg} obtained from biexponential (open symbols) and triexponential (closed symbols) fits to the PL decay traces. b) PL decay trace of a representative sample (red curve, NR9 in Table S1), and biexponential fit (black curve).

10. Comparison with literature lifetimes

In Figure 6b, the radiative lifetimes calculated for our samples are compared to literature data for CdSe NCs. Regarding the data from Gao and Peng[9], the core diameter was converted into the NC absorption peak energy using the calibration curve by Jasieniak,[8] and finally into the PL peak energy by applying a Stokes shift of 35.0 meV, which we estimated from our DiR dataset (Figure S13).

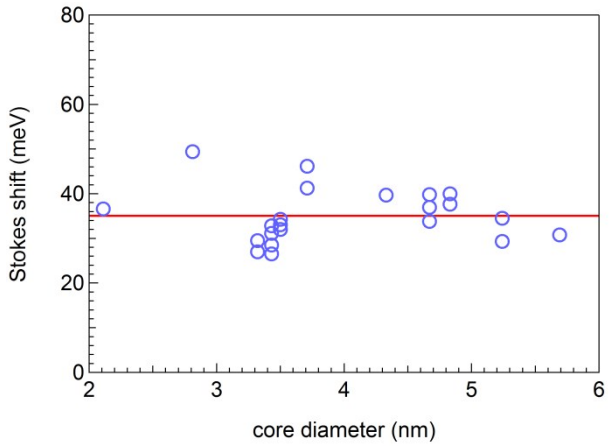

Figure S13. Stokes shift versus core diameter for our DiR samples. The red line is a linear fit to the data.

Data of De Mello Donegá,[10] Van Driel[11] and Gong[12] are given with respect to the PL peak energy or emission frequency, and were included as extrapolated from the graphs.

References

(1) Bohren, C. F.; Huffman, D. R. Absorption and Scattering by a Sphere. In *Absorption and Scattering of Light by Small Particles*; Wiley-VCH Verlag GmbH, 1998.

(2) Ninomiya, S.; Adachi, S. Optical Properties of Cubic and Hexagonal CdSe. *J. Appl. Phys.* **1995**, *78*, 4681–4689.

(3) Ninomiya, S.; Adachi, S. Optical Properties of Wurtzite CdS. *J. Appl. Phys.* **1995**, *78*, 1183–1190.

(4) Hens, Z.; Moreels, I. Light Absorption by Colloidal Semiconductor Quantum Dots. *J. Mater. Chem.* **2012**, *22*, 10406.

(5) Čapek, R. K.; Moreels, I.; Lambert, K.; De Muynck, D.; Zhao, Q.; Van Tomme, A.; Vanhaecke, F.; Hens, Z. Optical Properties of Zincblende Cadmium Selenide Quantum Dots. *J. Phys. Chem. C* **2010**, *114*, 6371–6376.

(6) Ricard, D.; Ghanassi, M.; Schanne-Klein, M. C. Dielectric Confinement and the Linear and Nonlinear Optical Properties of Semiconductor-Doped Glasses. *Opt. Commun.* **1994**, *108*, 311–318.

(7) Adachi S. *Optical Constants of Crystalline and Amorphous Semiconductors: Numerical Data and Graphical Information*; Springer Science & Business Media, 1999.

(8) Jasieniak, J.; Smith, L.; Embden, J. van; Mulvaney, P.; Califano, M. Re-Examination of the Size-Dependent Absorption Properties of CdSe Quantum Dots. *J. Phys. Chem. C* **2009**, *113*, 19468–19474.

(9) Gao, Y.; Peng, X. Photogenerated Excitons in Plain Core CdSe Nanocrystals with Unity Radiative Decay in Single Channel: The Effects of Surface and Ligands. *J. Am. Chem. Soc.* **2015**, *137*, 4230–4235.

(10) de Mello Donegá, C.; Koole, R. Size Dependence of the Spontaneous Emission Rate and Absorption Cross Section of CdSe and CdTe Quantum Dots. *J. Phys. Chem. C* **2009**, *113*, 6511–6520.

(11) van Driel, A. F.; Allan, G.; Delerue, C.; Lodahl, P.; Vos, W. L.; Vanmaekelbergh, D. Frequency-Dependent Spontaneous Emission Rate from CdSe and CdTe Nanocrystals: Influence of Dark States. *Phys. Rev. Lett.* **2005**, *95*, 236804.

(12) Gong, H.-M.; Zhou, Z.-K.; Song, H.; Hao, Z.-H.; Han, J.-B.; Zhai, Y.-Y.; Xiao, S.; Wang, Q.-Q. The Influence of Surface Trapping and Dark States on the Fluorescence Emission Efficiency and Lifetime of CdSe and CdSe/ZnS Quantum Dots. *J. Fluoresc.* **2007**, *17*, 715–720.